Proc. Natl. Acad. Sci. USA
Vol. 91, pp. 4859–4863, May 1994
Biophysics

A helical-dipole model describes the single-channel current rectification of an uncharged peptide ion channel

(minimalist protein design/α-helix/electrostatics/permeation/ion-channel asymmetry)

PAUL K. KIENKER, WILLIAM F. DEGRADO*, AND JAMES D. LEAR†

Du Pont Merck Pharmaceutical Co., Wilmington, DE 19880

Communicated by David Eisenberg, January 31, 1994

ABSTRACT **We are designing simple peptide ion channels as model systems for the study of the physical principles controlling conduction through ion-channel proteins. Here we report on an uncharged peptide, Ac-(Leu-Ser-Ser-Leu-Leu-Ser-Leu)$_3$-CONH$_2$, designed to form an aggregate of parallel, amphiphilic, membrane-spanning α-helices around a central water-filled pore. This peptide in planar lipid bilayers forms ion channels that show single-channel current rectification in symmetric 1 M KCl. The current at a given holding membrane potential is larger than the current measured through the same channel when the potential is reversed. Based on our hypothesized gating mechanism, the larger currents flow from the peptide carboxyl terminus toward the amino terminus. We present an ionic electrodiffusion model based on the helical-dipole potential and the dielectric interfacial polarization energy, which with reasonable values for dipole magnitude and dielectric constants, accurately replicates the current–voltage data.**

Many aspects of signal transduction and transmission in living cells depend on ionic currents, which flow into or out of the cell through ion-channel proteins. The currents of several types of channel have an asymmetric dependence on the transmembrane potential; if the larger current is directed toward the cell interior, the channel is said to be inwardly rectifying. Whole-cell rectification, arising from the summed currents of many individual channels, can arise from a difference in the channel opening–closing equilibrium at positive and negative membrane potentials (asymmetric voltage gating). However, a single open channel can also show rectification. This rectification can be caused by asymmetries in Mg^{2+} blocking (1–3), permeant ion concentration (4, 5), and fixed electrical charges or dipoles at the membrane surface or in the channel (6).

Both fixed charges and dipoles are likely to affect conduction in ion-channel proteins. Charge effects have been demonstrated in the nicotinic acetylcholine receptor, where single-channel conductance and rectification properties depend on the charge of certain amino acid side chains thought to be near the conducting pore (7). However, the effect of dipoles on conduction has not been as clearly demonstrated, even though they could be important in pores lined by α-helices. The dipole moments of the peptide bonds in an α-helix add together to form an electrical macrodipole (8, 9). Transmembrane α-helices are major structural features of membrane proteins such as bacteriorhodopsin (10) and the photosynthetic reaction center (11) and are thought to line the pores of ion channels such as the gap junction (12, 13) and the nicotinic receptor (14). [Dipoles might also influence rectification in channels without α-helices, such as certain forms of the model channel gramicidin (15, 16).]

The publication costs of this article were defrayed in part by page charge payment. This article must therefore be hereby marked "*advertisement*" in accordance with 18 U.S.C. §1734 solely to indicate this fact.

We are using minimalist-designed peptide ion channels to study the physical principles underlying conduction through protein ion channels. To study purely dipolar effects on rectification, we have designed and synthesized an uncharged amphiphilic peptide, Ac-(Leu-Ser-Ser-Leu-Leu-Ser-Leu)$_3$-CONH$_2$ [Ac-(LSSLLSL)$_3$] with the amino and carboxyl termini blocked by acetyl (Ac) and carboxamide (CONH$_2$) groups, respectively. Previous studies have indicated that the unacetylated homologue peptide H$_2$N-(Leu-Ser-Ser-Leu-Leu-Ser-Leu)$_3$-CONH$_2$ [(LSSLLSL)$_3$] is helical and forms voltage-gated, cation-permeable channels when incorporated into a planar lipid-bilayer membrane (17, 18). Molecular modeling of this sequence indicated that a parallel bundle of six α-helices has an 8-Å pore diameter, consistent with our data on the relative conductances of large organic cations (17) and with subsequent voltage-gating data (19). We base our Ac-(LSSLLSL)$_3$ model on this structure. We have not determined the single-channel rectification properties of (LSSLLSL)$_3$ channels, due to their short open-channel lifetimes and the steep voltage dependence of channel opening.

Here we present single-channel current–voltage data from channels formed by the Ac-(LSSLLSL)$_3$ peptide. We observe single-channel current rectification in this model system with no fixed charges on the peptide, no asymmetry in bathing ion concentrations, and no divalent cations. We propose a permeation model in which the dipole potential of parallel peptide helices generates the current asymmetry.

THEORY

A simple model describing the net flux of ions through a peptide channel in a lipid bilayer was constructed to provide a physical interpretation of our experimental results. We chose an electrodiffusion model in which ion concentration and electrical potential gradients within the membrane act as driving forces for the flow of ions across the membrane. Transfer of an ion from bulk water to a molecular-sized pore surrounded by a medium of low dielectric constant produces interfacial polarization; this result tends to reduce the ion concentration in the pore. With the same concentration of electrolyte on both sides of the pore, these effects must produce a symmetric (nonrectifying) current–voltage relation. Rectification occurs only if the pore contains an intrinsic source of asymmetry with respect to the direction of ion transmission. The parallel α-helical model for the Ac-(LSSLLSL)$_3$ channel predicts an intrinsic electrical asymmetry due to the alignment of the α-helical macrodipoles (8). This model consists of an aggregate of $n_h = 6$ parallel α-helical peptides about a cylindrical pore of radius $a = 4$ Å and length

Abbreviations: Ac-(LSSLLSL)$_3$, Ac-(Leu-Ser-Ser-Leu-Leu-Ser-Leu)$_3$-CONH$_2$; (LSSLLSL)$_3$, H$_2$N-(Leu-Ser-Ser-Leu-Leu-Ser-Leu)$_3$-CONH$_2$.

*To whom reprint requests should be addressed.
†Present address: Department of Biochemistry and Biophysics, University of Pennsylvania, Philadelphia, PA 19104.

L = 30 Å [assuming a coiled-coil pitch angle of 18° gives (1.5 Å)cos(18°) as the rise per residue (20, 21)]. We assume that the helical dipole determines the peptide orientation across the membrane, so that the amino terminus is on the negative-holding-potential side of the membrane, and the carboxyl terminus is on the opposite side (18). We further assume that the helices maintain this orientation as long as a particular channel remains open, even if the membrane potential changes during this period. We treat the potential $\phi(x, V)$ of an ion in the pore as the sum of three components: a constant-field component $\phi_c(x, V)$ arising from the applied transmembrane potential V, a helical-dipole potential component $\phi_h(x)$, and a dielectric interfacial polarization component (image energy) $\phi_i(x)$, where x is the distance along the pore axis, defined as 0 in the middle of the membrane, $L/2$ at the amino-terminal mouth, and $-L/2$ at the carboxyl-terminal mouth.

The helical-dipole potential can be approximated as the superposition of the potentials of a partial positive charge z_h at the peptide amino terminus and a partial negative charge $-z_h$ at the carboxyl terminus (9). The magnitude of the effective end charge valence is estimated to be between 0.5 and 0.75 charges (9); however, electrolyte screening can reduce the dipole potential, and hence the effective charge, if the helix termini are exposed to the solvent (22). (The unscreened value of the charge applies to the relative energies of a helix in two conformations; electrolyte screening does not affect energy differences if it stabilizes both conformations equally.) A model accounting for the detailed shape of the dielectric interface and electrolyte exclusion would be needed for a reliable calculation of the potential (23); in lieu of this we fit z_h as a free parameter.

Our approximation for the interfacial polarization potential is based on the calculations of Parsegian (24) and Jordan (25); our values for the peak image energy agree fairly with Jordan's value for pore diameters comparable to our model but deviate from his values for narrower pores. The model has two dielectric regions; dielectric constants are $\varepsilon_s = 80$ for the pore solution and the bulk aqueous solution and ε_l for the pore lining (which in our model is primarily peptide rather than lipid); $\varepsilon_l/\varepsilon_s$ defines the dielectric ratio K. The components of the potential are the applied transmembrane potential

$$\phi_c(x, V) = V(x + L/2)/L, \quad [1a]$$

the helical-dipole potential

$$\phi_h(x) = (z_h n_h e/4\pi\varepsilon_0\varepsilon_s) \times \{[a^2+(x - L/2)^2]^{-0.5} - [a^2 + (x + L/2)^2]^{-0.5}\}, \quad [1b]$$

and the interfacial polarization potential

$$\phi_i(x) = (e/4\pi\varepsilon_0\varepsilon_s) \times \{f(K)/a - \ln[2/(1 + K)]/(KL)\}\exp(-x^2/2\sigma^2), \quad [1c]$$

where e is the elementary charge, ε_0 is the permittivity of free space, $f(K)$ is defined in equation B3 of ref. 24, and σ is a parameter describing the shape of the interfacial polarization potential. [For simplicity we assume that K^+ is the only conductive species and represent the polarization energy as a potential. Preliminary experiments indicate that Ac-(LSSLLSL)$_3$ channels also have some Cl^- permeability (26); the possible consequences of ion–ion interactions in the pore are outside the scope of the present report.] We fit the current–voltage relations with a one-dimensional Nernst–Planck electrodiffusion model (27), in which the single-channel current is given by

$$I(V) = F\beta DAC[\exp(VF/RT) - 1]/\int_{-L/2}^{+L/2}\exp[\phi(x, V)F/RT]dx, \quad [2]$$

where K^+ has a partition coefficient $\beta = 1$, diffusion coefficient in the pore $D = 10^{-5}$ cm^2/s, and C is bulk molar activity. The pore cross-sectional area is $A = \pi a^2$, and F, R, and T are the Faraday constant, gas constant, and absolute temperature ($RT/F \approx 25.5$ mV at 23°C). In fitting the current–voltage data, we vary z_h, K, and σ.

MATERIALS AND METHODS

The Ac-(LSSLLSL)$_3$ peptide was synthesized by treating 10 mg of (LSSLLSL)$_3$ (17) with a 3-fold excess of the *N*-hydrosuccinimide ester of acetic acid (prepared by treating acetic acid with equimolar amounts of dicyclohexylcarbodiimide and *N*-hydrosuccinimide) and a 3-fold excess of diisopropylethylamine in 0.5 ml of dimethyl sulfoxide. The reaction proceeded to completion within several hours, and the product was purified by reverse-phase HPLC with a Hamilton PRP-1 column.

Bilayer membranes were formed by the monolayer-apposition technique (28) across a 50- to 80-μm hole in a Teflon film separating two Teflon chambers. The hole was pretreated with 10 nl of squalane dissolved in pentane. Squalane and pentane were purified on alumina N and A columns, respectively (ICN). A 2 mg/ml solution of the zwitterionic lipid 1,2-diphytanoyl-*sn*-glycero-3-phosphocholine (Avanti Polar Lipids) in pentane was added to the surface of the bathing solution 1–2 μl at a time. The lipid was purified by DEAE-cellulose chromatography (29). Membranes were formed by raising the bath levels using plastic syringes, and membrane capacitance was monitored on an oscilloscope using a triangle-wave voltage input. After a stable membrane formed, typically ≈300 pmol of peptide (lipid/peptide, 150:1, dissolved in methanol) was added to each of the bathing solutions; the membrane was then broken and reformed to incorporate peptide. (No differences were apparent in experiments with peptide added in lipid vesicles instead of methanol.) All experiments used bathing solutions of 1 M KCl "roasted" at 550°C/5 mM Hepes/0.2 mM EDTA, pH 7.0/KOH. All experiments were done at room temperature, 22–23°C. Membrane voltage was controlled, and currents were measured by using an EPC-7 patch-clamp amplifier (List/Medical Systems, Greenvale, NY), with a capacitance compensation circuit added [after Alvarez (30)], an 8-pole low-pass Bessel filter (Frequency Devices, Haverhill, MA), a LabMaster digital/analog converter, TL-1 interface, and model AI2020A event detector (Axon Instruments, Burlingame, CA). Because the peptide orientation in the membrane depends on the membrane potential, we adopt the sign convention that the holding potential is always negative. pCLAMP software (Axon Instruments) was modified so that voltage pulses or ramps could be triggered by the event detector, and the membrane current before and after the trigger event could be recorded. Episodes with no channel events were also acquired for later baseline subtraction. Currents were analyzed by using our modified pCLAMP software, and theoretical fits used the program MLAB (Civilized Software, Bethesda, MD).

RESULTS

Measurement of the rectification of single channels required channels of longer lifetime than those formed by the parent peptide, (LSSLLSL)$_3$. Assuming that the conducting state of (LSSLLSL)$_3$ was a parallel bundle of α-helices with positive

charges on the unblocked N termini of the helices, we reasoned that blocking the N termini might stabilize the conducting state (and hence increase channel lifetime) by reducing the electrostatic repulsion between neighboring helices. Thus, Ac-(LSSLLSL)$_3$ was designed to produce channels of longer lifetime.

Ac-(LSSLLSL)$_3$ Forms Voltage-Gated Channels. The voltage dependence of Ac-(LSSLLSL)$_3$ channel opening is qualitatively similar to that previously observed for (LSSLLSL)$_3$ channels: opening frequency increases with the magnitude of the holding potential (19). As expected, the open lifetimes of Ac-(LSSLLSL)$_3$ channels are longer than those of (LSSLLSL)$_3$ channels, with a mean of ≈200 ms at −200 mV, facilitating the use of voltage pulses and ramps. Fig. 1 shows single-channel current fluctuations vs. time induced by Ac-(LSSLLSL)$_3$ in 1 M KCl, pH 7, with a holding potential of −170 mV. Most of these channels have a current amplitude of about −23 ± 2 pA, although some smaller channels are evident (see Fig. 1) and, more rarely, larger channels are also observed. Here, we analyze only the predominant conductance state.

Ac-(LSSLLSL)$_3$ Channels Exhibit Single-Channel Current Rectification in Symmetric Bathing Solutions. Fast voltage pulses or voltage ramps (20 ms) were triggered during channel openings; channels often remained open long enough so that a complete single-channel current–voltage relation could be obtained (Fig. 2). The current–voltage data in Fig. 3 were obtained in one experiment by pulsing from a holding potential of −200 mV to the potential shown on the abscissa; four voltage-ramp experiments gave similar results. The current shows clear rectification; the single-channel current at −200 mV (−32 pA) was more than three times as large as the current at 200 mV (9 pA), and the slope conductance at −200 mV (285 pS) was about seven times as large as the conductance at 200 mV (40 pS). According to our gating model, the greater current flows from the channel peptide carboxyl terminus to the amino terminus. We occasionally observe channels with a greater or lesser degree of rectification than the predominant state, but they are too rare for systematic analysis.

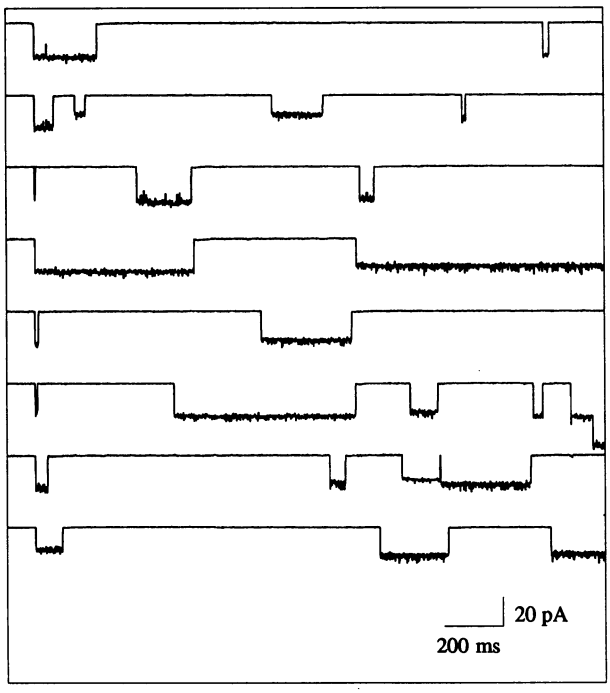

FIG. 1. Single-channel current recordings of Ac-(LSSLLSL)$_3$ channels in 1 M KCl, pH 7; channels open downward. Holding potential was −170 mV, and filter frequency was 500 Hz. (Bars = 20 pA vertical, 200 ms horizontal.)

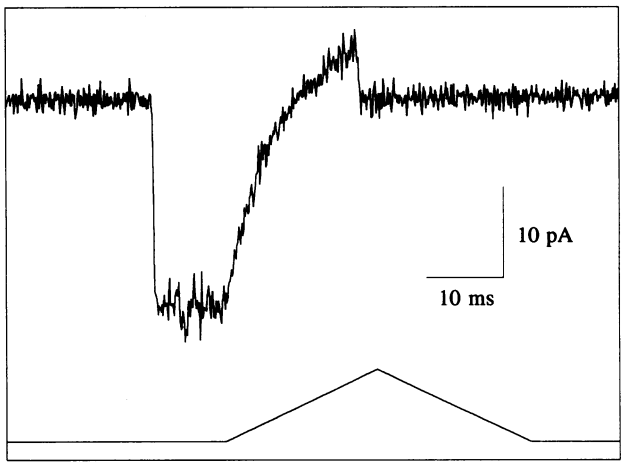

FIG. 2. Baseline-subtracted Ac-(LSSLLSL)$_3$ single-channel current (upper trace) and membrane potential (lower trace) vs. time, during a voltage ramp triggered by the channel opening. During the ramp the voltage increases from −170 mV to 170 mV and then decreases back to −170 mV. The initial downward current deflection is a channel opening; the channel current during the increased voltage ramp appears as a curving segment. The channel closes near the end of the increased voltage ramp. Filtering was 2 kHz. [Bars = 10 pA vertical (upper trace), 10 ms horizontal (both traces).]

The Helical-Dipole Potential Quantitatively Accounts for the Rectification. The solid curve in Fig. 3 shows the best fit of the electrodiffusion model (Eqs. 1 and 2) to the data. The adjustable parameters (obtained through nonlinear least-squares fitting) are the effective helix end charge valence z_h = 0.122, the pore lining/solution dielectric ratio K = 0.149, and interfacial polarization potential width parameter σ = 12.4 Å. The fitted helical-dipole and interfacial-polarization potential profiles $\phi_h(x)$ and $\phi_i(x)$ (Eq. 1b and 1c) and their sum, $\phi_{hi}(x)$, are plotted in Fig. 4, together with a representative constant-field potential component $\phi_c(x)$ (Eq. 1a); the peak values of $\phi_h(x)$, $\phi_i(x)$, and $\phi_{hi}(x)$ are 1.1, 2.2, and 2.3 RT/F, respectively. Only that part of the total potential between ±15 Å is used to calculate the current. If the fit is repeated using a larger effective pore radius (a = 5.5 Å vs. 4 Å in the above calculation), to account for the distance from the edge of the pore to the peptide backbone, the current–voltage curve is fit as well as before, but requiring (primarily)

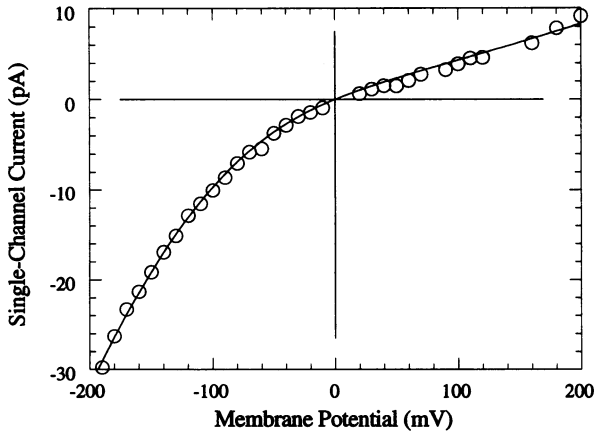

FIG. 3. Averaged Ac-(LSSLLSL)$_3$ single-channel current–voltage data (○). Currents from 96-voltage pulses, from a holding potential of −200 mV to the potential indicated on the abscissa, contributed to the graph. Filtering was 2 kHz. The solid curve is a fit of the electrodiffusion model of Eqs. 1 and 2 using z_h = 0.122, K = 0.149, and σ = 12.4 Å.

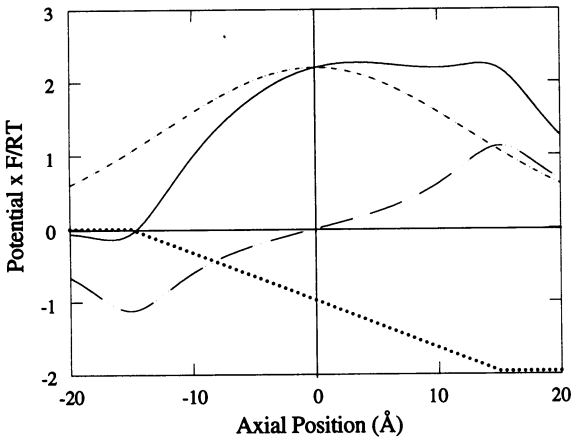

FIG. 4. Fitted-potential profile for a cation passing along the Ac-(LSSLLSL)$_3$ pore axis. ——, Helical-dipole potential $\phi_h(x)$; – – –, interfacial polarization potential $\phi_i(x)$; solid curve, the sum $\phi_{hi}(x)$. A representative constant-field potential component $\phi_c(x)$ is also shown (···), representing a −50 mV transmembrane potential.

a reduction in the dielectric ratio (actual fit parameters were $z_h = 0.161$, $K = 0.057$, and $\sigma = 13.0$ Å).

DISCUSSION

In previous studies we have postulated that the (LSSLLSL)$_3$ and (LSLLLSL)$_3$ family of peptides form channels consisting of parallel bundles of α-helices. This model predicts that the single-channel currents should rectify in symmetric bathing solutions, which is born out by the present experiments. The rectification is well described by a simple three-parameter electrodiffusion model. Furthermore, the fitted values of the parameters are physically reasonable and close to the values expected from theory. The fitted value of the dielectric ratio K makes the pore-lining dielectric constant $\varepsilon_1 \approx 12$, in the range expected for a narrow pore lined with neutral, amphiphilic peptides (22). The effective helix end charge valence z_h, accounting for electrolyte screening with the Debye–Hückel model, is predicted to be

$$z_h = z_0 \exp(-\kappa a), \qquad [3]$$

where $z_0 = 0.5$ is the effective charge valence in the absence of electrolyte, and the Debye length $1/\kappa$ is 3.2 Å in 1 M KCl (31). For pore radius $a = 4$ Å, Eq. 3 predicts $z_h = 0.143$, near the fitted value of $z_h = 0.122$. Finally, the fitted value of the interfacial polarization potential width parameter, $\sigma = 12$ Å, accords well with calculations on more realistic ion-channel models (25).

Preliminary experiments indicating that rectification is more pronounced at lower [KCl] also support a role for electrolyte screening (unpublished data). The conductance–KCl activity relation appears linear at zero and positive membrane potentials (up to 1 M KCl concentration) and only weakly sublinear at negative membrane potentials, supporting the use at this stage of a model without ion–ion interactions.

The model we have proposed is consistent with the current–voltage data; however, not surprisingly, other models with asymmetric potential profiles can also fit the data. Factors other than the helical-dipole potential could contribute to conductance asymmetry in helical-aggregate pores. Examples include amino acid side-chain orientation or order in the sequence, a funnel-shaped pore, or specific ion-binding characteristics of the helix end groups. Some elementary examples of alternative asymmetric potential profiles giving reasonable fits to our data are as follows: (*i*) a rectangular plateau of height 2.2 RT/F between $x = -8.3$ Å and $x = 15$ Å; (*ii*) a triangular potential with a peak of 3.5 RT/F at $x = 7.5$ Å; and (*iii*) a model with surface potentials of 0.7 RT/F at $x = -15$ Å and 2.7 RT/F at $x = 15$ Å. (Some of these fits are not optimal but could be improved by varying the K^+ permeability parameter βD.) All of these potential profiles have one common feature: the potential is, on average, more positive for $x > 0$ (toward the putative amino-terminal side) than for $x < 0$ (toward the putative carboxyl-terminal side).

The condition for "amino-ward" rectification (larger currents from carboxyl terminus to amino terminus than from amino terminus to carboxyl terminus) is that $I(V) < -I(-V)$, for all $V > 0$. Upon substituting from Eq. 2 and making use of the relation $\phi_c(x, V) = V + \phi_c(-x, -V)$, this condition becomes

$$\int_{-L/2}^{+L/2} \exp\{[\phi_c(x, V) + \phi_{hi}(x)]F/RT\}dx > \int_{-L/2}^{+L/2} \exp\{[\phi_c(x, V) + \phi_{hi}(-x)]F/RT\}dx, \qquad [4]$$

for $V > 0$. From this we can see that a (positive) potential profile $\phi_{hi}(x)$ skewed toward the amino terminus ($x > 0$) produces "amino-ward" rectification; a profile skewed toward the carboxyl terminus ($x < 0$) produces "carboxyl-ward" rectification, and only a symmetric profile can generate a symmetric current–voltage curve. A more intuitive explanation for the cause of rectification relies on the relative directions of the two driving forces for ion flux: the ionic concentration gradient and the potential gradient. If the voltage-independent component of the potential profile $\phi_{hi}(x)$ is most positive toward the amino terminus, the cation concentration will be lowest there, so cations diffusing down their concentration gradient will tend to flow from carboxyl terminus to amino terminus. This "amino-ward" diffusive flux may be paired with either a supporting or an opposing electrically driven flux. A negative membrane potential drives cations from carboxyl to amino terminus, adding to the diffusive flux, whereas a positive membrane potential drives cations from amino to carboxyl terminus, against the diffusive flux. Hence the negative, "amino-ward" current is greater in magnitude than the positive, "carboxyl-ward" current.

The effect of the helical-dipole potential on protein folding and catalysis has been extensively studied in water-soluble proteins (9), and some work has been done in membrane proteins (32), but relatively little study has been given to its role in conduction through ion channels. "Tilted" helical dipoles have been suggested to influence charge selectivity in alamethicin (33). Two groups have calculated the effect of the helical dipole on the energies of proton or electron transport through the interior of a helix but only briefly considered ion passage through a helix-lined pore (34, 35). It has been calculated that the helical-dipole potential of the five parallel M2 segments thought to line the nicotinic receptor channel should create an energy barrier of 85 RT, which would prevent ion conduction, were it not compensated by the potential of fixed charges or other helices (36). Our model, for six parallel helices around a pore of comparable radius, does not indicate such a large energetic barrier. The key difference in the models appears to be the treatment of the effective dielectric constant inside the pore.

It is thought that each M2 segment of the nicotinic receptor has its amino terminus toward the inside of the cell and its carboxyl terminus toward the extracellular side (7, 37); on this basis our model predicts inward rectification. This is, in fact, observed for the nicotinic receptor in symmetric solu-

tions of monovalent ions with negligible concentrations of divalent cations (38). The helical-dipole potential could, therefore, play a role in nicotinic receptor rectification, although, as previously demonstrated, other factors such as fixed charges must certainly contribute to the overall potential profile (7).

In conclusion, the results of this paper show the power of minimalist protein design to illuminate fundamental physical processes affecting protein structure and function. Although it had been expected that the helical-dipole potential contributes to ion translocation and rectification (36), the multiplicity of other steric and electrostatic effects in complex natural proteins had made it impossible to experimentally determine the magnitude of this effect. Through the use of structurally simple models, however, it is now possible to study the helical dipole in isolation and to test and refine quantitative models of its effect on ion-channel function.

Thanks go to Sharon Jackson for preparing and purifying Ac-(LSSLLSL)$_3$, to Dick Mahlangu for preliminary measurements of its channel properties, to Zelda Wasserman for spirited discussions, to Daniel Camac for technical advice and lipid purification, to Bob French for technical advice, and to Maria Rafalski for help in translating ref. 34. This research was supported, in part, by the Office of Naval Research.

1. Horie, M., Irisawa, H. & Noma, A. (1987) *J. Physiol. (London)* **387**, 251–272.
2. Matsuda, H., Saigusa, A. & Irisawa, H. (1987) *Nature (London)* **325**, 156–159.
3. Vandenburg, C. A. (1987) *Proc. Natl. Acad. Sci. USA* **84**, 2560–2564.
4. Goldman, D. E. (1943) *J. Gen. Physiol.* **27**, 37–60.
5. Hodgkin, A. L. & Katz, B. (1949) *J. Physiol. (London)* **108**, 37–77.
6. Frankenhaeuser, B. (1960) *J. Physiol. (London)* **152**, 159–166.
7. Imoto, K., Busch, C., Sakmann, B., Mishina, M., Konno, T., Nakai, J., Bujo, H., Mori, Y., Fukuda, K. & Numa, S. (1988) *Nature (London)* **335**, 645–648.
8. Wada, A. (1976) *Adv. Biophys.* **9**, 1–63.
9. Hol, W. G. J. (1985) *Prog. Biophys. Mol. Biol.* **45**, 149–195.
10. Henderson, R. & Unwin, P. N. T. (1975) *Nature (London)* **257**, 28–32.
11. Deisenhofer, J. & Michel, H. (1989) *EMBO J.* **8**, 2149–2170.
12. Unwin, N. (1989) *Neuron* **3**, 665–676.
13. Tibbitts, T. T., Caspar, D. L. D., Phillips, W. C. & Goodenough, D. A. (1990) *Biophys. J.* **57**, 1025–1036.
14. Unwin, N. (1993) *J. Mol. Biol.* **229**, 1101–1124.
15. Busath, D. & Szabo, G. (1981) *Nature (London)* **294**, 371–373.
16. Durkin, J. T., Providence, L. L., Koeppe, R. E., II, & Andersen, O. S. (1993) *J. Mol. Biol.* **231**, 1102–1121.
17. Lear, J. D., Wasserman, Z. R. & DeGrado, W. F. (1988) *Science* **240**, 1177–1181.
18. Chung, L. A., Lear, J. D. & DeGrado, W. F. (1992) *Biochemistry* **31**, 6608–6616.
19. Åkerfeldt, K. S., Lear, J. D., Wasserman, Z. R., Chung, L. A. & DeGrado, W. F. (1993) *Acc. Chem. Res.* **26**, 191–197.
20. Crick, F. H. C. (1952) *Nature (London)* **170**, 882–883.
21. Dunker, A. K. & Zaleske, D. J. (1977) *Biochem. J.* **163**, 45–57.
22. Honig, B. H., Hubbell, W. L. & Flewelling, R. F. (1986) *Annu. Rev. Biophys. Biophys. Chem.* **15**, 163–193.
23. Gilson, M. K. & Honig, B. H. (1988) *Proteins: Struct. Funct. Genet.* **3**, 32–52.
24. Parsegian, V. A. (1975) *Ann. N.Y. Acad. Sci.* **264**, 161–174.
25. Jordan, P. C. (1986) in *Ion Channel Reconstitution*, ed. Miller, C. (Plenum, New York), pp. 37–55.
26. Kienker, P. K., DeGrado, W. F. & Lear, J. D. (1993) *Biophys. J.* **64**, 371 (abstr.).
27. Hille, B. (1992) *Ionic Channels of Excitable Membranes* (Sinauer, Sunderland, MA), p. 345.
28. Montal, M. & Mueller, P. (1972) *Proc. Natl. Acad. Sci. USA* **69**, 3561–3566.
29. Kates, M. (1972) *Techniques of Lipidology: Isolation, Analysis and Identification of Lipids* (North-Holland, Amsterdam), pp. 408–411.
30. Alvarez, O. (1986) in *Ion Channel Reconstitution*, ed. Miller, C. (Plenum, New York), pp. 115–130.
31. Robinson, R. A. & Stokes, R. H. (1968) *Electrolyte Solutions* (Butterworth, London), p. 78.
32. Krishtalik, L. I., Tae, G.-S., Cherepanov, D. A. & Cramer, W. A. (1993) *Biophys. J.* **65**, 184–195.
33. Hall, J. E., Vodyanoy, I., Balasubramanian, T. M. & Marshall, G. R. (1984) *Biophys. J.* **45**, 233–247.
34. Ovchinnikov, A. A. & Ukrainskii, I. I. (1979) *Dokl. Akad. Nauk SSSR* **244**, 751–754.
35. Van Duijnen, P. T. & Thole, B. T. (1981) *Chem. Phys. Lett.* **83**, 129–133.
36. Eisenman, G., Villaroel, A., Montal, M. & Alvarez, O. (1990) *Prog. Cell Res.* **1**, 195–211.
37. Leonard, R. J., Labarca, C. G., Charnet, P., Davidson, N. & Lester, H. A. (1988) *Science* **242**, 1578–1581.
38. Dani, J. A. & Eisenman, G. (1987) *J. Gen. Physiol.* **89**, 959–983.